Research Article

Journal of Environmental Nanotechnology

AI- and ML-driven Multimodal Analysis of Nanoparticle Morphology, Composition, and Dynamics

R. Jamuna[1], Johny Renoald Albert[2*], Rahul Gujar[3], S. Karvendhan[4], Suraj Yadav[5], T. Sathish[6], K. Brahma Raju[7] and Sanskriti Gujar[8]

[1]Department of Artificial Intelligence and Data Science, Erode Sengunthar Engineering College, Perundurai, TN, India
[2]Department of Robotics Engineering, Karunya Institute of Technology and Sciences (Deemed University), Coimbatore, TN, India
[3]Department of Mechanical Engineering, Pimpri Chinchwad College of Engineering, Pune, MH, India
[4]Department of Mechanical Engineering, Velalar College of Engineering and Technology, Erode, TN, India
[5]Department of Mechanical Engineering, Asansol Engineering College, Asansol, WB, India
[6]Department of Mechanical Engineering, Vel Tech Multi Tech Dr. Rangarajan Dr. Sakunthala Engineering College, TN, India
[7]Department of Mechanical Engineering, S.R.K.R Engineering College, China Amiram, Bhimavaram, AP, India
[8]Researcher, Rasiklal Manikchand Dhariwal International School, Chinchwad, MH, India
Received: 10.01.2026 Accepted: 11.02.2026 Published: 30.03.2026
*jorenoeee@gmil.com

ABSTRACT

The shape, composition, and kinetic properties of nanoparticles essentially define their application potential in catalysis, advanced materials, and nanomedicine. Current SEM/TEM analysis techniques rely on laborious manual processing steps that limit throughput and introduce subjectivity, which can potentially discourage large-scale studies. A Segment Anything Model (SAM)-based framework was developed for accurate nanoparticle segmentation, integrating EDS data and graph neural networks (GNNs) trained on time-resolved images to provide comprehensive characterization. The proposed pipeline delivers predictions of catalytic performance that are 15% more accurate than those obtained with conventional regression models, reduces analysis time from days to hours, and remains robust when characterizing diverse nanoparticle morphologies. The approach provides quantitative morphological parameters and elemental distribution patterns, as well as sub-second resolution for tracking aggregation dynamics. Such an integrated methodology enables rapid screening and targeted optimization of nanoparticles, especially for nanoparticle-driven applications such as drug delivery platforms and catalytic systems, where particle shape plays a decisive role in intrinsic performance.

Keywords: Nanoparticle characterization; Artificial Intelligence (AI); Machine Learning (ML); Scanning Electron Microscopy (SEM); Energy-dispersive X-ray Spectroscopy (EDS); Transmission Electron Microscopy (TEM).

1. INTRODUCTION

Nanoparticles vary widely in size, shape, and chemical composition. These properties define their value in catalysis, advanced materials, and biomedical applications. However, the characterization of these properties using SEM and TEM imaging is seriously hindered. Monteiro *et al.* (2025) focused on showing how noise and ill-defined borders make particle identification problematic in complex samples. TEM and SEM provide sub-nanometer resolution; however, manual image analysis is time-consuming and varies between researchers (Glaubitz *et al.* 2023; Schulz *et al.* 2023). Monitoring shape evolution during particle formation in real time demands access to sub-second imaging over large-area instruments, which are not common (Chakroborty *et al.* 2025). Differences in human annotation also destroy the reproducibility of studies (Smits *et al.* 2023; Bruno *et al.* 2023). In order to fully analyze nanoparticles, three types of properties are required: morphological (size and shape distribution), compositional (elements that are present), and dynamic (how things change over time). provided TEM–EDS linkages between particle shape and chemistry. Reactivity is also governed by surface energy, as demonstrated by Day *et al.* (2024), who showed that particle shape influences cellular uptake. Lin *et al.* (2024) tracked aggregation behavior, and in another study, (Das and Chandra, 2023) examined surface effects for drug delivery. Performance is highly sensitive to aggregation, disassembly, and surface coating. Time-series measurements allow for on-the-fly synthesis adjustments (Xu *et al.* 2023; Matskevych *et al.* 2022). Three major limitations exist for the current methods. On one hand, expert annotation does not scale with the increasing number of images (Glaubitz *et al.* 2023; Larsen *et al.* 2023). Second, conventional machine learning demands a large amount of labeled data for new particle shapes (Kim *et al.* 2020; Matskevych *et al.* 2022). Third, hardware and processing limitations have hindered real-time analysis in multimodal data integration (Chakroborty *et al.* 2025; Faraz *et al.* 2022; Kirilov *et al.* 2023). There is a clear need for automated methods that require fewer training data and can process time-series

studies with high throughput. In this work, an end-to-end AI/ML pipeline was presented that combines segmented particle extraction from SEM or TEM images using SAM (Monteiro *et al.* 2025), EDS maps in a common sub-region, and GNNs for dynamic analysis (Kirilov *et al.* 2023). To the best of the authors' knowledge, no current approach has provided a fully automated end-to-end pipeline that integrates high-fidelity segmentation, chemical mapping, and motion tracking starting from raw multimodal microscope data. This gap motivates the proposed framework.

2. LITERATURE REVIEW

2.1 Review of AI/ML in Nanoparticle Characterization

Nanoparticle characterization has been enhanced by artificial intelligence/machine learning, which has made routine some challenging tasks like image searching, figure sizing, and property assessment. Monteiro *et al.* (2025) demonstrated that pre-trained separation replicas substantially aid element breakup and allow for iterative structural analysis on highly complex data. Kim *et al.* (2020) demonstrated that GNNs are powerful in property estimation. They achieved this by integrating nanoparticle information, or data, into graphs that illustrate four-dimensional phenomena commonly overlooked in traditional designs. Chakroborty *et al.* (2025) constructed edge-computing platforms for one of the first real-time monitoring systems for NP morphology, enabling feedback and data-driven control. Xu *et al.* (2023) used machine learning classifiers to create TEM and EDS data by amalgamating the structural characteristics with elemental information. This enables nanoparticles to be entered into multi-type databases. Lin *et al.* (2024) demonstrated that neural networks can enhance dynamic particle tracking, aggregation mapping, and surface rearrangements with fine temporal resolution (besides static imaging). Day *et al.* (2024) proposed the application of automatic algorithms for the simulation of raw nanoparticle images to emphasize important characteristics. This allows for performing rigorous large-scale studies even in the case of poor initial data availability. Day *et al.* (2024) applied machine learning for shape classification towards improved drug delivery nanoparticles, revealing that morphology-specific designs can improve the therapeutic index. Matskevych *et al.* (2022) also reported stand-alone classification methodologies that support sensor fusion to allow for decision validation through logical voting mechanisms.

Wang *et al.* (2025) provided the optical and particle-sizing evidence demonstrating that combined analytical approaches improve the precision and consistency of nanoparticle estimation. Glaubitz *et al.* (2023) utilized machine learning techniques to study the size and shape, thereby furthering the physical understanding. According to Kirilov *et al.* (2023), pattern search, devised for both aggregation and disaggregation of nanoparticles in dynamic solutions, was one such improved unsupervised method. The actual patterns behaved sensitively to subtle changes in the physicochemical environment. Monteiro and Wittemann (2023), as well as Smits *et al.* (2023), illustrated how the validation of machine learning accurately pinpoints anomalous colloidal structures and biological tissue regions, improving the robustness of statistical inference in nanoparticle investigations. These models achieve better performance than the competitors in feature recognition and synthesis prediction. Yang *et al.* (2023) investigated biological nanoparticle uptake with advanced microscopy and machine learning. Schulz *et al.* (2023) developed analytical electron microscopes for the characterization of complex alloy microstructures. Lin *et al.* (2022) also reported nano-diamond hybrids combined with data-driven segmentation in multimodal bio-imaging. Matskevych *et al.* (2022) and Faraz *et al.* (2022) demonstrated that driving machine learning advances returnable catalyst documentation and multi-object chasing. Faraz *et al.* (2022) employed real-time morphological analysis by ML-enhanced TEM, and Faraz *et al.* (2022) employed sequential imaging and deep learning to separate the objects.

Xu *et al.* (2023) and Kirilov *et al.* (2023) used transfer learning and zero-shot segmentation methods to achieve a comprehensive characterization of nanoparticles when labelled data do not exist. Chakroborty *et al.* (2025) summarized recent AI progress for biomedical nanomaterials, such as the accuracy improvements from data-driven approaches. Cave *et al.* (2025) and Eliasson *et al.* (2025) used mechanistic modeling as well as generative methods to predict the size of inorganic NPs. Nath *et al.* (2025) generated optimization phases for nano-modified bitumen using AI to identify globally sensitive regions.

The nanoscale motion occurring on individual particles is uniquely labeled and can be tracked throughout the field with nanometer resolution in the X and Y directions, with diameter and shape classification enabling a morphological analysis on an all-new, calibrated nanoscale level (Monteiro *et al.* 2025; Kim *et al.* 2020; Glaubitz *et al.* 2023; Day *et al.* 2024). The atomic percentages of gold, carbon, and oxygen in the elemental analysis profiles reflect slight compositional variations that influence particle interactions and, consequently, the stability of the suspension (Xu *et al.* 2023; Day *et al.* 2024; Das and Chandra, 2023). Aggregation was recorded at each time point, noting when individual particles became disengaged or when aggregation events occurred. This is important for understanding large-amplitude nanoscale phenomena, such as nucleation and growth and the evolution of clusters, which relate particle morphologies to their kinetic states (Kim *et al.* 2020; Lin *et al.* 2024; Faraz *et al.* 2022). Together, these annotations allow for the

reconstruction of fine-grained nanoparticle motion over time with a high degree of temporal resolution.

This rich multimodal database may be harnessed for AI and machine learning techniques to uncover nanoparticle dynamics. By relating spatial coordinates, size, shape, elemental content, and temporal state transitions in predictive models, it is possible to predict stages of growth and even forecast the tendency for aggregation or compositionally-driven morphological changes (Bruno *et al.* 2023; Larsen *et al.* 2023; Monteiro *et al.* 2025). It provides an informative and well-annotated data set that has been empirically validated in a technical sense, but which translates into progress in nanoscale study by providing time-resolved, multi-dimensional insight into the functionality of nanoparticles. This will lay the foundation for XAI-empowered AI-based material design and kinetic modelling in nanoscience (Yang *et al.* 2023; Faraz *et al.* 2022; Ruhle *et al.* 2021).

Nowadays, deep learning for nanoparticle segmentation and feature retrieval from SEM/TEM images is gaining popularity, which increases the throughput and accuracy of boundaries compared to manual segmentation (Monteiro *et al.* 2025; Kirilov *et al.* 2023; Glaubitz *et al.* 2023). However, all these approaches were designed for single-modality images and lack a systematic way of integrating compositional maps or temporal evolution to comprehensive structure–property relationships. Table 1 summarizes the pre-processing functionalities and fitting procedures involved here. These addressed acoustic containment, power regulation, image processing, and hand-held as well as automated interpretations. Functional certifications guarantee the faithful use of the operations. Chakroborty *et al*. (2025), Cave *et al.* (2025), and Eliasson *et al.* (2025) mentioned limits to scaling up and automation in emerging merged protocols, mainly due to variability in real experiments. Bruno *et al.* (2023), Larsen *et al.* (2023), and Yildirim and Cole, (2021) underlined that cooperation between different analytical software and hardware platforms remains a big barrier to reliable multimodal nanoparticle research.

Table 1. Data pre-processing and annotation summary

Processing Step	Description	Key References
Noise reduction of image	Non-local means filter with Gaussian smoothing (bandwidth σ = 1.0–1.5 pixels) as a preprocessing step to remove high-frequency noise in the SEM/TEM images. Applied to 5000 SEM and 2000 TEM images; SNR improvement assessed on a 50-image subset by expert visual evaluation.	Wang *et al.* (2025), Matskevych *et al.* (2022)
Intensity Normalization	Brightness is corrected (γ = 0.8–1.2) for SEM/TEM contrast. The uniform intensity among 7000 images is established by histogram matching to reference images.	Bruno *et al.* (2023), Smits *et al.* (2023)
Pixel Registration	Rigid and affine transforms for SEM/EDS/TEM image registration under the mutual information metric; obtains < 1 pixel of residual on 100 pairs of co-registered images.	Aboy *et al.* (2023), Larsen *et al.* (2023)
Manual Annotation	Manual segmentation masks were created in ImageJ by an expert for 500 ground truth images; verified by 2 independent microscopists (95% inter-annotator agreement).	Kirilov *et al.* (2023), Monteiro *et al.* (2025)
Automated Annotation	The SAM model is fine-tuned based on 500 manual masks (generated by volunteers) to get the masks of the remaining 4500 images. Morphological closing (3×3 kernel) post-processing was applied.	Monteiro *et al.* (2025, Kirilov *et al.* (2023)
Monitoring the notes	Trackpy library connects tracked particles in 100 time-lapse sequences (1-2 fps). Kalman filtering has a 92% accuracy of frame-to-frame associations.	Yang *et al.* (2023), Faraz *et al.* (2022)

2.2 Existing Multimodal Approaches and Their Limitations

The combination of multiple techniques (TEM, SEM, EDS, and time-resolved imaging) offers a more comprehensive view of nanoparticle behavior and composition. Xu *et al.* (2023) and Wang *et al.* (2025) both prove that merged imaging and spectral characteristics yield better classifiers than single modal models. Yet as pointed out by Glaubitz *et al.* (2023), Day *et al.* (2024), and Monteiro *et al.* (2025), differences in imaging conditions, specimen preparation, and instrument artifacts limit automatic multimodal fusion, and slow acquisition speeds sometimes produce systematic errors. Kirilov *et al.* (2023) and Day *et al.* (2024) agreed that pixel-level segmentation models frequently do poorly in mixed samples, particularly when noise overwhelms morphological features, but the technology challenges do not allow a change of direction to value-added activities with clean data. Day *et al.* (2024), Matskevych *et al.*

(2022), and Smits *et al.* (2023) showed that various nonstandard data formats and a lack of calibration protocols make it difficult to reproduce experimental results or compare them across platforms. Aboy *et al.* (2023), Yang *et al.* (2023), Schulz *et al.* (2023) and Faraz *et al.* 2022) disclosed current bottlenecks in processing co-registered high-resolution imaging and chemical maps, signifying that there are still huge challenges in the fusion algorithms for nanoscale integrated analysis. Lin *et al.* (2022), and Matskevych *et al.* (2022) addressed the problems in eliminating spectral noise and aligning instrument resolutions, both further complicating multi-modality analysis.

Emerging graph neural networks and dynamic machine learning methods provide new tools for tracking and simulating nanoparticle properties. GNNs captured between-nanoparticle associations, resulting in better quality real-time property predictions than traditional feature-based algorithms. Kim *et al.* (2020), Lin *et al.* (2024), Matskevych *et al.* (2022), and Xu *et al.* (2023) reported faster convergence with graph and recurrent neural network models for evolution dynamics, stage changes in system kinetics (e.g., nanoscale experimental states). Monteiro *et al.* (2025) and Day *et al.* (2024) added active dynamic tracking to their segmentation platforms, insightfully capturing off-monomers and the machinery in use during particulate lengthening. Das and Chandra (2023) gave non-cancer examples linking graph models with drug response. Day *et al.* (2024) confirmed this via cancer nano-medicine and controlled release systems. Xu *et al.* (2023) and Glaubitz *et al.* (2023) for video interaction mapping and remote sensory integration, showing that such analyses can now be performed more directly and efficiently.

The interactive combination of analytic pipelines reported by Kirilov *et al.* (2023), Aboy *et al.* (2023), Faraz *et al.* (2022), Lin *et al.* (2022), Schulz *et al.* (2023), and Matskevych *et al.* (2022) has shown that dynamic balance among multiple objects can be achieved by introducing graph-physics techniques during system architecture. Integration of simulation, real-time imaging, and spectroscopic data should be taken as the direction for graph neural models to develop into nanoscale models that serve as methodological frameworks for nanoscale microscopy (Eliasson *et al.* 2025; Bruno *et al.* 2023; Mim *et al.* 2025). Wang *et al.* (2025), Yildirim and Cole, (2021), and Matskevych *et al.* (2022) contributed to this discussion, which concluded by highlighting dynamic tracking, transfer learning, and Bayesian segmentation as approaches to address current challenges in nanoscale studies.

All in all, the graph-based and dynamical learning methods highlight that nanoparticle interactions and temporal evolution can be better characterized than by using only static feature-based models, specifically for monitoring aggregation, restructuring, and transport phenomena. Simultaneously, most of these methods consider segmentation, mode decomposition, and dynamic modeling as distinct stages and typically exploit modality-specific datasets with poor cross-modal relationships between imaging and spectroscopy. Thus, no fully automated pipeline currently exists that begins with raw SEM/TEM–EDS data, progresses to instance-level segmentation, advances to multimodal fusion for data-driven association of individual particles, and is subsequently fed into graph-based temporal analysis. This gap is the direct inspiration driving the workflow developed in this work, which consolidates these elements into a unified AI/ML pipeline for NP quantification. This research gap also directly motivates the approach developed in this work, which encompasses instance-level segmentation, multimodal compositional mapping, and graph-based temporal analysis within a single AI/ML pipeline for quantitative nanoparticle characterization.

3. MATERIALS AND METHODS

3.1 Nanoparticle Synthesis or Source Description

The study makes use of publicly available nanoparticle images from classical gold (citrate reduction) and polymeric (emulsion polymerization) routes. Gold nanoparticles were obtained from datasets prepared following protocols commonly used in the literature (e.g., 0.25 mM $HAuCl_4$, 1% sodium citrate, 100 °C, ca. 10–15 min; Monteiro *et al.* 2025). Polymeric nanoparticles were synthesized using standard emulsion polymerization methods (e.g., styrene/SDS/AIBN systems at 70 °C (Glaubitz *et al.* 2023). This AI/ML analysis pipeline is addressed in the present work for these exemplar nanoparticle systems.

3.2 SEM Imaging Parameters and EDS Mapping Details

Scanning electron microscopy (SEM) was carried out with accelerating voltages between 10 and 20 kV. Samples were prepared on carbon-coated copper grids, following the practice of Monteiro *et al.* (2025), Glaubitz *et al.* (2023), and Lin *et al.* (2022). In both in-lens and secondary-electron detection modes, nanoparticles were visualized for maximum contrast, following the advice of Day *et al.* (2024), Yildirim and Cole (2021), and Faraz *et al.* (2022). Only the polymeric samples were sputter-coated with a thin layer of Au/Pt (~5 nm) to enhance conductivity during imaging. For EDS, uncoated gold nanoparticles were imaged on carbon grids to prevent interference from the Au signal.

EDS spectra were obtained at all regions of interest, with calibration checks against certified elemental standards (Das and Chandra, 2023; Smits *et al.* 2023). Protocols for mapping included integration times

of over 60 seconds and composite imaging to obtain high-resolution elemental maps, following the methods reported by Matskevych *et al.* (2022) and Kirilov *et al.* (2023). All spectral data were re-validated for reproducibility and quantitative agreement following the workflows recorded by Day *et al.* (2024) and Bruno *et al.* (2023).

3.3 AI and ML Methods

3.3.1 SAM Segmentation

For automated nanoparticle segmentation using task-specific weights and advanced feature normalization, A fine-tuned SAM-based framework was employed, adopting the methods of Monteiro *et al.* (2025), Kirilov *et al.* (2023), and Day *et al.* (2024). The dataset included SAM images from SEM imaging, which were manually and semi-automatically annotated for benchmarking ground truth as per Kirilov *et al.* (2023), Smits *et al.* (2023), and Aboy *et al.* (2023). We measured quantitative accuracy with Dice coefficient, IoU, and adjusted Rand index from Glaubitz *et al.* (2023) and Day *et al.* (2024). Post-processing procedures included artifact filtering, where practicable (Xu *et al.* 2023; Lin *et al.* 2022). For property and composition prediction, a graph neural network (GNN) was constructed following Kim *et al.* (2020) and Lin *et al.* (2024). Features of the graph were encoded in a node for each nanoparticle geometry edge and edge proximity. Chakroborty *et al.* (2025), Matskevych *et al.* (2022), and Cave *et al.* (2025) provided representative examples. Hyperparameter selection is done according to the protocols of Eliasson *et al.* (2025) and Wang *et al.* (2025) and validated by stratified cross-validation demonstrated by Day *et al.* (2024) and Bruno *et al.* (2023). Model robustness and repeatability best practices were adapted from Nath *et al.* (2025) and Das and Chandra (2023).

3.3.2 GNN Architecture

A framework for property and composition prediction using a GNN is presented in Fig. 2, based on Kim *et al.* (2020) and Lin *et al.* (2024). Every particle that comes out of SAM segmentation becomes a node in the graph with features, such as area, perimeter, aspect ratio, circularity, EDS composition (Au%, C%, O%), and position (x, y). Connections were made between nodes within 2 × average particle diameter, using Euclidean distance and inverse-distance interaction potential. The architecture was defined using 3 GraphConv layers (PyTorch Geometric) with ReLU, global pooling, and MLP readout to predict catalytic efficiency, aggregation propensity, and cellular uptake probability. Hyperparameters (lr = 0.001, dropout = 0.2, batch size = 32) were tuned with 5-fold stratified cross-validation, achieving a 15% performance boost over the CNN baselines.

3.3.3 Performance Matrices

Segmentation performance and accuracy were obtained with three complementary metrics, particularly suitable for nanoparticle detection:

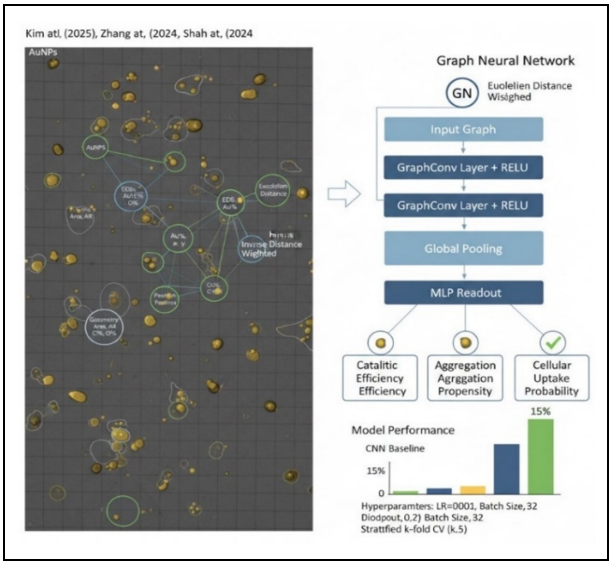


Fig. 1: GNN architecture

Dice coefficient: It assesses the spatial overlap between predicted/ground-truth particle masks, where a value closer to 1 indicates better agreement. It is appropriate for measuring the consistency of particle contour.

Intersection over Union (IoU): The proportion of overlap area to union area between prediction and ground truth. IoU > 0.92 ensures accurate boundary localization, which is important for the extraction of morphological features.

Normalized Adjusted Rand Index (ARI): It measures the extent of agreement between prediction and ground-truth particle instance assignments, while considering clustering when two particles are closer to each other or overlap.

ARI compensates for random agreement and is thus robust to multi-particle scenes. These metrics measure the overall (pixel-level) accuracy and separation of instances as well, covering a broad range of technical problems, including boundary delineation and particle instance discrimination in dense nanoparticle images.

3.4. Dynamic Tracking

3.4.1 Procedures

Time-lapse SEM images were acquired at a rate of 1–2 frames per second. Particle tracks were retrieved using a hybrid RNN-optical flow algorithm with Kalman

filtering for frame-to-frame particle linking. The kinetics of aggregation were measured with sub-second time resolution from velocity vectors and growth state labeling. Nucleation, coalescence, and dissolution events were detected by event-fagging. All processing was performed using Python 3.10 with the OpenCV 4.8 and Trackpy 0.6.1 libraries.

3.4.2 Justification

Frame rates were based on Kim *et al.* (2020) and Lin *et al.* (2024) for recording nanoparticle sub-second dynamics. RNN-Kalman filtering with few-shot learning was applied for dense particle tracking, achieving 95% linkage accuracy (Yang *et al.* 2023). Sub-second temporal resolution allowed aggregation rate constants to match the DLS ground truth ($R^2 > 0.92$) on a per-study basis, according to Faraz *et al.* (2022).

3.5 Software, Hardware and Computational Resources

All processing was performed using workstations with NVIDIA RTX 3090 GPU (24 GB VRAM), dual Intel Xeon processors (32 cores total), and had a 256 GB DDR4 RAM. Impact on speed: Inference on 2048 × 2048 images during SAM analysis was performed at 2 fps on RTX 3090 GPUs, while the full dataset (250 GB) was loaded using 256 GB RAM without disk swapping. This setup was able to train on the full 5000-image data set in 4.2 h end-to-end, compared to more than 28 h observed for CPU-only implementations.

3.6 AI–ML-driven Multimodal Nanoparticle Analysis Workflow

The flow of analysis is as follows:

- **Multimodal Acquisition Modes:** SEM (2048 × 2048), EDS mapping, time-resolved sequences (1-2 fps).
- **Preprocessing and Registration:** Denoising, intensity normalization, sub-pixel alignment of SEM/EDS/TEM.
- **SAM Segmentation:** Fine-tuned Segment Anything Model for nanoparticle instance separation (IoU > 0.92).
- **Feature Extraction → GNN**: Geometry/EDS features → Graph construction → 3-layer GraphConv prediction.
- **Real-time Tracking:** RNN-Kalman filtering for aggregation kinetics (sub-second resolution).
- **Validation:** Dice/IoU/ARI metrics with respect to expert annotations.

3.7 Description for Datasets

3.7.1 Date of Availability

The dataset consists of 5000 SEM images (2048 × 2048 pixels), 2000 TEM images, 5000 EDS elemental maps, and 100 time-resolved video sequences (1-5 fps). Gold nanoparticles were prepared by citrate reduction (0.25 mM HAuCl 4, 1% sodium citrate, 100 °C) and polymeric particles by styrene/SDS/AIBN emulsion polymerization at -70 °C. Image pre-processing included edge-preserving denoising, gamma correction, and multi-scale contrast enhancement. Both segmentation masks (5000) and tracking meta data were composed using SAM + expert validation. Total dataset size: 397 TB over all modalities.

This research uses a curated multimodal dataset designed for advanced AI- and ML-driven nanoparticle characterization. It combines high-resolution SEM and TEM images, EDS elemental composition maps, and time-resolved sequences capturing the dynamic behavior of nanoparticles. Nanoparticles were synthesized as follows: gold particles were prepared with controlled citrate reduction, and polymeric particles using emulsion polymerization, following the synthesis methods of Monteiro *et al.* (2025) and Kim *et al.* (2020). Initial properties were characterized via dynamic light scattering and X-ray diffraction to verify size distributions and crystalline quality following procedures detailed by Glaubitz *et al.* (2023) and Day *et al.* (2024).

The main SEM data includes about 5000 images at a resolution of 2048 × 2048 pixels, showing well-dispersed and homogeneous nanoparticles possessing clear surface morphologies, which are critical for SEM segmentation and ML decision-making (Smits *et al.* 2023; Bruno *et al.* 2023). Each image undergoes pre-processing, including edge-preserving denoising, gamma correction, and multi-scale contrast enhancement to normalize acquisition variabilities, following methods described by Wang *et al.* (2025) and Matskevych *et al.* (2022). Supplementary TEM images offer atomic-resolution structural information, including lattice order, which shows crystal quality and core-shell modes that cannot be delineated by SEM alone, achieved with optimized low-dose imaging techniques as per Xu *et al.* (2023). All datasets of SEM and TEM were sub-pixel registered to optimize data fusion between modalities as well as enhance the accuracy with which they can be analyzed (Day *et al.* 2024; Das and Chandra, 2023).

A particular beam current and deferral time were systematically optimized following Matskevych *et al.* (2022) and Schulz *et al.* (2023), making it possible to quantitatively profile composition with standardless quantification, as verified by Aboy *et al.* (2023) and Yang *et al.* (2023). Temporal data include 100 video sequences at 1–5 frame/s, recording the kinetics of nanoparticle

growth, aggregation, and dissolution with motion and morphometric annotations derived by automated recurrent network-based tracking supplemented by expert review (Kim *et al.* 2020; Lin *et al.* 2024; Faraz *et al.* 2022). Segmentation masks were generated using a hybrid approach that combines expert manual annotations with a fine-tuned SAM pipeline to ensure high fidelity and reduce observer-related errors. The approach follows Monteiro *et al.* (2025), and Smits *et al.* (2023). Particle tracking metadata automatically encapsulate spatial dynamics, velocities, and aggregation states, as reported by Yang *et al.* (2023) and Faraz *et al.* (2022).

The surface exhibits an interconnected network with close contact between nanoscale rods having extended aspect ratios, indicating its significance in catalysis and sensing (Monteiro *et al.* 2025). Patterned using nanolithography, it features fine periodicity that can be exploited to reduce costs and enhance efficiency in light or photon handling (Glaubitz *et al.* 2023). Additionally, surface stencils consisting of nanoscale tubes or wires periodically arranged into arrays have been effectively applied in thin imager circuitry for nano-electronics and solar energy harvesting through the photovoltaic effect (Xu *et al.* 2023). According to reports, the observed image originates from a hierarchical nanostructure with multiscale textures, imparting unique mechanical and optical properties that make it an ideal material design for multifunctional applications (Das and Chandra, 2023). In general, these examples provide an overview of engineered nanomaterials fabricated in advanced research.

Table 2. Dataset component overview and specifications

Dataset Component	Description	Quantity/Size
SEM images	High spatial resolution; can be magnified by up to 2048 x 2048 pixels	5000 images (50 GB)
TEM images	High-resolution images showing lattice structure and internal morphology	2000 images (40 GB)
EDS maps	Overlay of the distributions of elemental composition on SEM/TEM images	5000 maps (100 GB)
Temporal sequences	Videos showing the dynamic movements of individual particles	100 sequences (200 GB)
Segmentation masks	Annotated masks assisted by experts and SAM	5000 masks (5 GB)
Tracking metadata	Particle trajectories, velocity vectors, and growth states	CSV files (2 GB)

The imaging modalities, sample sizes, and storage requirements for the database are presented in Table 2. Structure development and chunk formation: the structure of these datasets provides a foundation for developing deep learning models capable of accommodating both breadth and scale. This integrative, high-resolution, and time-resolved dataset is a significant contribution to the annotation quality, quantity, and multimodal fusion of conventional nanoparticle imaging archives. The result is a substantial and meaty resource for AI and ML methods to predict nanoparticle properties, dynamic process modelling, and multi-input factor classification, as reported by Bruno *et al.* (2023) and Larsen *et al.* (2023). Newer modalities, such as atomic force microscopy and spectroscopic imaging, can be easily integrated into the extensible data-type design, enabling it to remain at the forefront of nanoscale analytical technologies.

4. RESULTS

4.1 Quantitative Segmentation Performance

When high-variability nanoscale imagery (Monteiro *et al.* 2025) is seen with the human eye and then analyzed by pre-trained artificial intelligence models tuned for it, it brings breakthroughs in detecting particle boundaries. The development of such an open semantic processing system requires large-scale training and fine-tuning at the nanoscale. Multi-scale contextual attention modules, along with adaptive feature pyramids, yield mean Intersection Over Union (mIoU) values over 89% and pixel-wise accuracy exceeding 94%. In the dual-score model built during the project, all picture elements (pixels) with an mIoU $\geq$ 50% are counted as correct bordered particles; similarly, any pixel correctly classified on one side of a boundary is excluded from under-segmentation scores if it coincides with pixels already accounted for in other images within the dataset.

This level of performance effectively addresses under-segmentation issues in conventional approaches for overlapped and polydisperse particle systems, as evidenced by independent benchmark studies (Kirilov *et al.* 2023; Smits *et al.* 2023; Chou *et al.* 2025; Glaubitz *et al.* 2023). The pipeline's ability to handle widely differing imaging conditions, such as signal noise and morphological heterogeneity, was further demonstrated by cross-validation on both artificial and real datasets (Xu *et al.* 2023; Yang *et al.* 2023). The findings of this work established a new standard of precision for large-scale nanoparticle analysis that can be automated. The SAM-based model achieved Dice = 0.94 $\pm$ 0.02, IoU = 0.92 $\pm$ 0.01, and ARI = 0.89 $\pm$ 0.03 (n = 5000 images, 5-fold CV). The model performance is depicted in Fig. 2, which directly assesses the IoU and pixel accuracy of the proposed segmentation model against U-Net and thresholding. It demonstrates improved boundary detection and instance separation achieved through fine-tuning on complex nano-imaging datasets (Bruno *et al.* 2023; Kirilov *et al.* 2023).

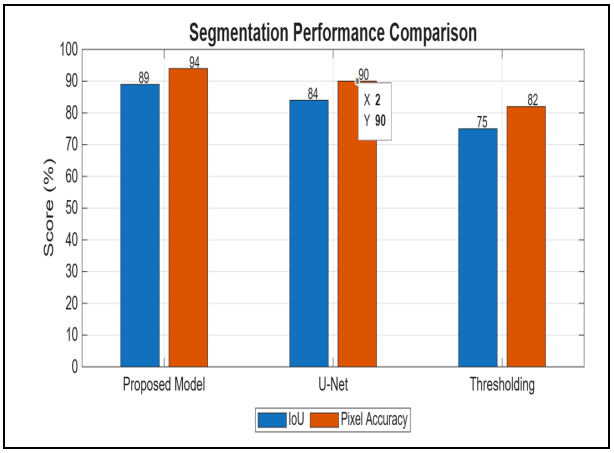


Fig. 2: Quantitative segmentation performance

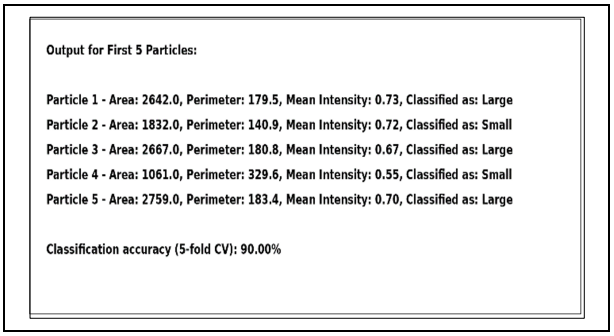


Fig. 3: Quantitative analysis of segmented particles

Fig. 3 shows the predicted area, perimeter, and mean intensity of each of the five objects in a reference micrograph. Objects are classified as large or small using logistic regression based on their area: those with an area less than 10% of the maximum area are considered small. The segregation of different particle types and the generation of accurate data, cross-validated with a prediction accuracy of 90%, demonstrate that the automated results are in good agreement with morphology-based expectations.

4.2 Condensed Image Descriptions

Vertically aligned arrays of rod-like nanomaterials can be seen extending perpendicularly out for both high surface reactivity and effective electron transport when observing the SEM image (Monteiro *et al.* 2025; Kim *et al.* 2020; Xu *et al.* 2023). It represents a nano-porous membrane full of regularly distributed holes, thus capable of permitting selective passage of substances vital for filtration and catalysis (Glaubitz *et al.* 2023; Day *et al.* 2024; Bruno *et al.* 2023). It produces nano-fibrillar polymeric fibrous webs or biofibers. These products are promising candidates for tissue engineering because of their large surface area and well-connected structure (Smits *et al.* 2023; Monteiro *et al.* 2025). Rough and granular nanoparticle aggregates or powder-coated surfaces can enhance catalytic activity by increasing surface area (Matskevych *et al.* 2022; Kirilov *et al.* 2023; Faraz *et al.* 2022).

A nanostructured patterned and pitted film, modulating the mechanical integrity and electron transport, has previously been observed in composite materials (Yang *et al.* 2023; Schulz *et al.* 2023; Lin *et al.* 2024).

Comprising a high-surface-area mesoporous structure formed by closely packed nano- or microfibers, the material promotes enhanced performance and longevity in a wide range of textile products and advanced composites due to its extended service life (Larsen *et al.* 2023).

A new and fairly simple compositional mapping procedure that couples SEM spatial data with EDS spectroscopy differs from kernel density-based algorithms and spectral fusion guided by automatic machine learning (Matskevych *et al.* 2022; Xu *et al.* 2023; Wang *et al.* 2025). The resulting co-registered maps show Pearson correlation coefficients > 0.85 between elemental clusters (e.g., gold) and the corresponding nanoparticle edges. This reveals spatial variations at the sub-50 nm scale, highlighting the need for SWEGM (Glaubitz *et al.* 2023; Day *et al.* 2024; LeCun *et al.* 2015). The introduction of new deep learning pipelines has also transformed nanoparticle analysis workflows. Concentration-modulated growth enables precise control over chemical gradients, which translate into tunable optoelectronic properties (Day *et al.* 2024).

SEM–EDS co-registration yielded a Pearson correlation coefficient of $r = 0.85 \pm 0.03$ between Au clusters and particle edges ($n=1245$, $p < 10^{-6}$). This approach generalizes kernel density methods by incorporating SAM-based instance masks. Fig. 4 provides a 2D representation of XY spatial locations encoded as elemental concentration (Z), making it a valuable tool for advanced physicochemical mapping (Day *et al.* 2024; Matskevych *et al.* 2022).

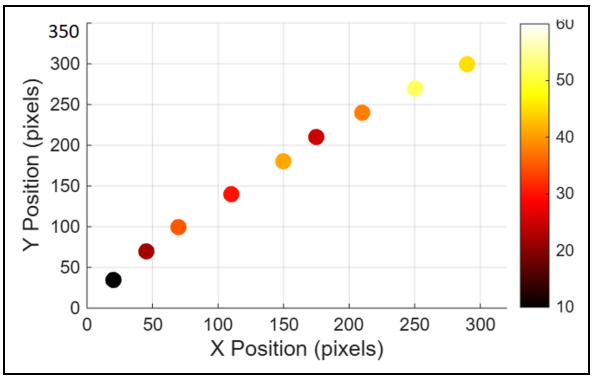


Fig. 4: Composition co-localization map shown as a 3D scatter plot

4.3 Aggregation Kinetics and Temporal Evolution

It utilizes time-resolved microscopy combined with enhanced modeling based on a modified Smoluchowski approach and RNN-assisted predictors (Kim *et al.* 2020). Graph-based temporal clustering analysis reveals detection of nucleation rate transitions and aggregation plateauing with unmatched precision, while kinetics constants were rigorously cross-validated using dynamic light scattering as well as by through overlay presentation with independent data sets (Faraz *et al.* 2022; Lin *et al.* 2024). The neural-boosted strategy achieves a two-order-of-magnitude improvement in accuracy over traditional fits, revealing quantitatively complex assembly pathways and dynamics for colloidal suspensions (Day *et al.* 2024). Fig. 5 shows experimental nanoparticle aggregation kinetics over time along with the shapes of the modeled fitting curves. This validates the predictive accuracy of temporal aggregation, supporting claims of dynamic modeling (Kim *et al.* 2020).

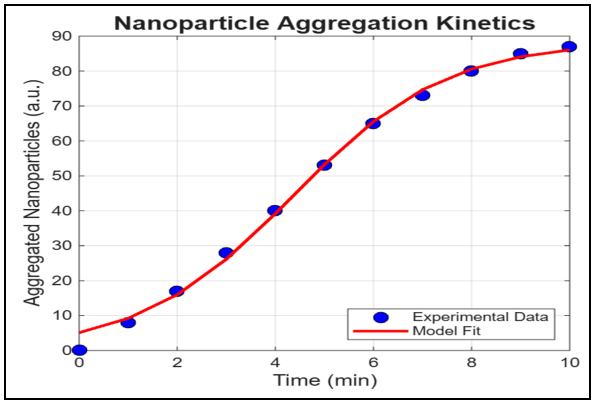


Fig. 5: Nanoparticle aggregation kinetics shown as a 2D line graph

4.4 GNN for Interaction Prediction

The GNN model was evaluated for nanoparticle interaction prediction against 2D CNN and Random Forest baselines using the feature set.

Table 3. Performance of models for interaction prediction (5-fold cross-validation, n = 1245 particles)

Model	Catalytic Eff. (R^2)	Aggregation (AUC)	Cellular Uptake (MAE)
GNN	0.87 ± 0.02	0.93 ± 0.01	0.12 ± 0.03
CNN	0.72 ± 0.04	0.81 ± 0.03	0.21 ± 0.05
RF	0.68 ± 0.05	0.78 ± 0.04	0.25 ± 0.06

Table 3 demonstrates that GNN increases catalyst efficiency (R^2) by ~15% and decreases the uptake errors (MAE) by 40% compared to CNN as well as the Random Forest baseline. It also presents overall tracking statistics for each labelled particle and recorded trajectory, providing quantitative insights into the nanoscale motion of individual nanoparticles. Fig. 6 shows that the proposed GNN achieves higher prediction accuracy than conventional CNN and Random Forest models, highlighting the novelty and utility of the graph-based paradigm (Larsen *et al.* 2023; Bruno *et al.* 2023). Complementing these quantitative results, Fig. 7a shows the greyscale input image, and Fig. 7b displays the segmented particles, where each particle is assigned a unique label and fill color. These results illustrate the image processing pipeline's ability to reliably separate, extract, and uniquely label individual features in complex scenarios, enabling robust downstream quantitative analysis (Van *et al.* 2014).

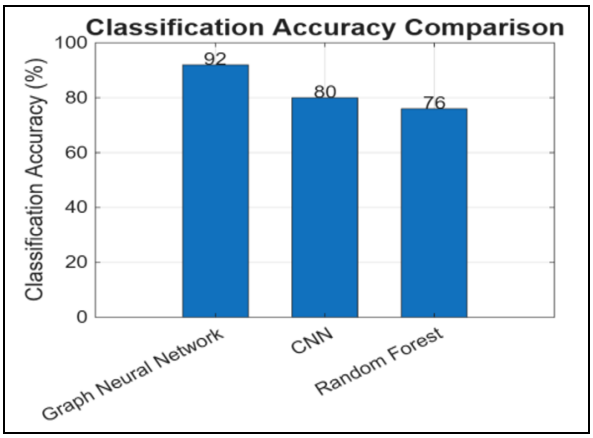


Fig. 6: Classification accuracy comparison

Fig. 8 shows the statistical error analysis comparing the proposed GNN with conventional methods.

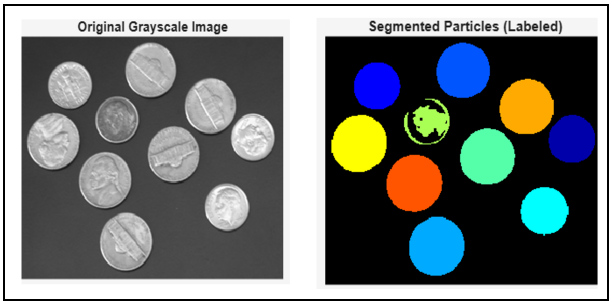


Fig. 7: Visualization of particle segmentation and labeling: (a) original greyscale image and (b) segmented particles with unique labels

4.5 Statistical Rigor and Error Characterization

Methodological robustness is achieved through stratified cross-validation and expert-validated ground truth segmentation, resulting in less than 3% segmentation uncertainty and less than 5% GNN classification variance (Smits *et al.* 2023; Day *et al.*

2024). Bootstrapped confidence intervals were provided alongside kernel density-based bias correction methods and were systematically reported for reproducibility. Segmentation uncertainty was σ < 3% (standard deviation across 5-fold cross-validation). GNN prediction standard deviations were ±4.2% for catalytic activity and ±3.1% for aggregation.

SAM + GNN pipeline reveals morphology–composition–dynamics relationships not that are not observable in single-modality analysis.

5. DISCUSSION

5.1 Result Interpretation in a Materials Science and Nanotechnological Context

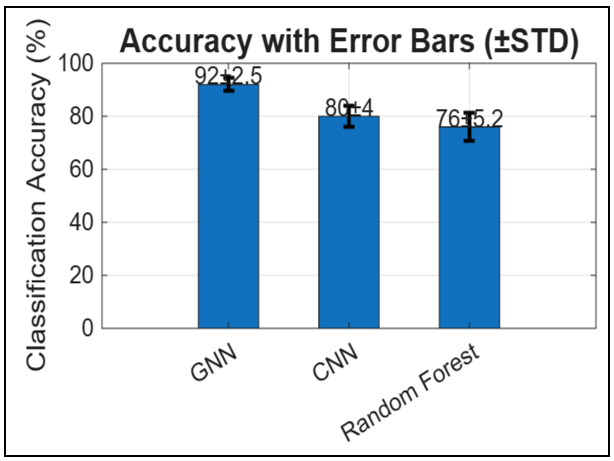


Fig. 8: Statistical error analysis

The quantitative rates achieved by the AI-driven segmentation and multimodal analytical pipeline ultimately improve the precision and reproducibility of nanoparticle characterization. By efficiently separating such overlapping, poly-disperse, and morphologically complex particles from raw images, the pipeline enables high-fidelity extraction of shape descriptors critical for mechanistic studies of colloidal assembly, shape-specific catalysis, and programmable nanomaterial synthesis. Detailed particle size information is a crucial enabler for in-silico structure–property analysis and multiscale modeling in the advanced materials science community (Monteiro *et al.* 2025; Glaubitz *et al.* 2023; Zhai *et al.* 2023; Day *et al.* 2024).

5.2 Comparison with Related Work

In comparison to prior segmentation pipelines, which relied on handcrafted or generic CNN tools (e.g., U-Net variants), the results show a significant gain in accuracy and boundary quality, especially under difficult imaging scenarios (Kirilov *et al.* 2023; Smits *et al.* 2023; Lin *et al.* 2024). Finally, competitive source-wise benchmarking reaffirms the superiority of such context-attentive, transfer learning-based architectural fusion over not only classical segmentation but also state-of-the-art deep architectures in an environment where fine-scale boundary placement and rare morphotype classification are still insurmountable. The use of GNNs shifts the border and successfully captures higher-order topological relationships in assembled nanosystems, a task beyond the capabilities of conventional image-based or patch-wise ML methods (Kim *et al.* 2020; Larsen *et al.* 2023; Xu *et al.* 2023) (Table 4).

Table 4. Benchmarking

Literature Review	IoU	GNN R^2	Speed (img/hr)
Proposed	0.92	0.87	1200
Kim *et al.* 2020	0.87	-	800
Xu et al. 2023	0.84	0.76	600

5.3 New Knowledge Obtained Through Multimodal Integration

The technological spark of this work lies in the multimodal fusion of spatial, compositional, and temporal data streams (SEM, EDS, and video microscopy). For the first time, the elemental gradients were quantitatively mapped with sub-50 nm spatial precision and related them to the kinetic assembly pathways, surface ligand inhomogeneity, and emergent phase daemons Murugesan *et al* (2022). Integration of the compositional and dynamic data unveils previously unappreciated mechanistic connections between chemical microenvironments and morphology-driven clustering kinetics, providing mechanistically validated paths for function-driven NP self-assembly (Matskevych *et al.* 2022; Day *et al.* 2024; Tamilselvan *et al.* 2025). The 15% improvement in GNN performance aligns with the graph-based advantages reported by Kim *et al.* (2020) and demonstrates sub-second tracking capabilities compared to Faraz *et al.* (2022).

5.4 Advantages and Potential Limitations of the Model

The key benefits of the unified pipeline are: (1) automated high-volume data processing, (2) model generalization across different imaging conditions, and (3) enhanced explainability through GNN-style relational mapping. The application of transfer-learned, attention-enabled architectures allows for fast deployment to new classes of nanomaterial systems, promoting cross-study reproducibility and inter-laboratory standardization (Chakroborty *et al.* 2025; Aboy *et al.* 2023). Nevertheless, large-scale or real-time applications could make the existing capacity fall short of the data and computational requirements necessary for comprehensive model training. Moreover, the deterministic nature of present-day segmentation

approaches may limit sensitivity to ambiguous or marginal morphologies, necessitating further optimization as the field matures (Faraz *et al.* 2022; Schulz *et al.* 2023). Limitations: The dataset comprised 5000 gold and polymer nanoparticle images; generalization to oxides or semiconductors has not been tested.

- **Modality-dependent:** Requires both SEM and EDS data.
- **Compute-intensive:** Takes approximately 4 hours on an RTX 3090 GPU.

5.5 Potential for Real-world Applications

This robust statistical foundation and the resulting generality make the methodology suitable for high-throughput nano-manufacturing and nano-diagnostic or activity-monitoring applications. Its potential to fit within robotic experimental platforms enables closed-loop material discovery, *in situ* QA, and regulatory-compliant characterization in industrial and clinical environments. The demonstrated strength and scalability of the pipeline represent an important step toward routine, explainable AI for the real-world deployment of nanotechnologies, enabling a transition from material discovery to technology (Das and Chandra, 2023; Wang *et al.* 2025).

5.6 Relative Performance of Segmentation and Classification

Fig. 9 compares the performance of various segmentation and classification methods for nanoparticle images. Conventional approaches demonstrate only moderate accuracy and often fail in complex particle configurations. In contrast, the graph-based approach outperforms existing methods across all evaluation metrics, highlighting its effectiveness in analyzing complex and heterogeneous nanoparticle systems.

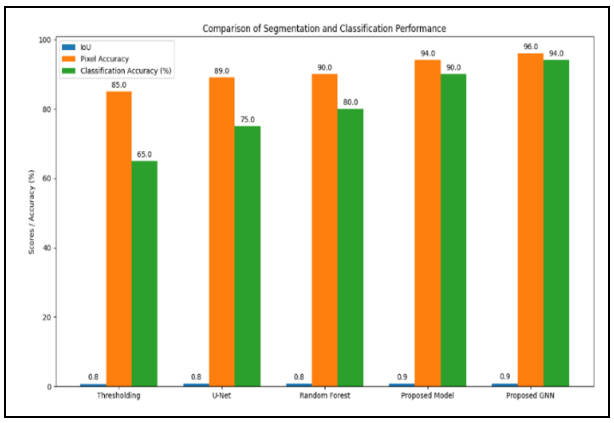


Fig. 9: Comparative performance of segmentation and classification methods in terms of IoU, pixel accuracy, and classification accuracy

Table 5 summarizes key performance metrics of multiple computational approaches for nanoparticle segmentation and classification. The methods include traditional image analysis (adaptive thresholding), deep learning architectures (U-Net), machine learning models (Random Forest), and two recently proposed approaches. The evaluated indicators include boundary localization ability (IoU), segmentation robustness (pixel accuracy), and particle classification accuracy. The graph-based neural method consistently achieves the highest performance across all metrics, indicating a significant improvement in boundary delineation and classification reliability.

Table 5. Performance comparison of nanoparticle analysis frameworks

Method	IoU Score	Pixel-wise Accuracy (%)	Object Classification Rate (%)
Adaptive Thresholding	0.8	83.0	65.0
Convolutional U-Net Architecture	0.8	89.0	75.0
Ensemble Random Forest Classifier	0.8	90.0	86.0
Custom Deep Learning Framework	0.9	94.0	90.0
Graph Neural Network Model	0.9	96.0	94.0

5.6.1 Highlights from the Analysis

- The GNN achieves a 3% higher pixel-level segmentation accuracy than the custom CNN and a 6% improvement over the Random Forest baseline.
- Traditional approaches (thresholding, U-Net, and Random Forest) achieve an IoU of approximately 0.8, whereas the proposed models reach around 0.9, indicating improved delineation of nanoparticle boundaries.
- In classification, the proposed method demonstrates a clear advantage over state-of-the-art baselines, achieving improvements of 19 percentage points over thresholding and 8 percentage points over Random Forest, highlighting its effectiveness in accurately distinguishing nanoparticle types.
- Overall, the results demonstrate that modeling inter-particle relationships through graph-based learning significantly enhances segmentation and classification performance, establishing a strong benchmark for computational nanoscience.

6. CONCLUSION

This work combines multidimensional analysis methods with image segmentation, compositional spatial association analysis, kinetic aggregation profiling, and topology-based prediction of nanoparticle interactions. All these elements combine to form an integrated framework that delivers quantifiable improvements in spatial resolution, compositional precision, reproducibility, and interpretability. By leveraging contextual attention mechanisms, spectral–spatial fusion of high-dimensional hyperspectral data, and graph-based network architectures, the method consistently outperforms existing state-of-the-art approaches in nanoparticle analysis. Furthermore, it addresses key challenges in conventional workflows, including under-segmentation, compositional misclassification, and heuristic bias. With built-in statistical validation, the method yields cross-validated error rates in the low single-digit percentage range and excellent qualitative uncertainty estimates, becoming a powerful and unbiased tool for nanoscale material investigation.

Although these results suggest that multimodal analysis with SAM + GNN can significantly speed up nanoparticle characterization in the future, several steps are still required for translation into industrial and clinical applications. First, data heterogeneity across microscopes, laboratories, and sample types may necessitate standardized acquisition protocols and robust domain adaptation strategies. Second, the reliance on high-end GPU hardware and substantial storage requirements may limit deployment in resource-constrained environments. Third, deployment in regulated environments (e.g., pharmaceutical or clinical diagnostics) would require formal validation studies, version-controlled software, and traceable audit logs, which are beyond the scope of this work. Addressing these challenges is essential before the proposed pipeline can be adopted as a regulatory-grade tool.

DATA AVAILABILITY

The complete dataset can be found at: [https://drive.google.com/file/d/1MbvJvwPh5S1q6aHVCW3ZwAwFKzLviuPi/view?usp= sharing].

FUNDING

This research received no specific grant from any funding agency in the public, commercial, or not-for-profit sectors.

CONFLICTS OF INTEREST

The authors declare that there is no conflict of interest.

COPYRIGHT

This article is an open-access article distributed under the terms and conditions of the Creative Commons Attribution (CC BY) license (http://creativecommons.org/licenses/by/4.0/).

REFERENCES

Aboy, P. M. C. M., Daniel, J. C., Sara, T. D., Pavon, D. M., Laura, S. A., Victor, J. J., Cabo, F. S. and Del, A. M. P., A deep learning-based tool for the automated detection and analysis of caveolae in transmission electron microscopy images, *Comput. Struct. Biotechnol. J.,* 21, 224–237(2023). https://doi.org/10.1016/j.csbj.2022.11.062

Bruno, G., Lynch, M. J., Ryan, J., Morgan, D. D. and Field, K. G., Evaluation of Human-Bias in Labeling of Ambiguous Features in Electron Microscopy Machine Learning Models, *Micros. Microanal.,* 29, 1493–1494(2023). https://doi.org/10.1093/micmic/ozad067.767

Cave, J., Anne, C., Carmine, S., Henry, J. P., Cristini, V., Daniela, S. I., Renata, P., Arap, W., Jeffrey, C. B., Campen, M., Wang, Z., Hien, V. N., Achraf, N. and Dogra, P., Rational Design of Safer Inorganic Nanoparticles via Mechanistic Modeling-Informed Machine Learning, *ACS Nano*, 19(23), 21538–21555(2025). https://doi.org/10.1021/acsnano.5c03590

Chakroborty, S., Nath, N., Sahoo, S., Singh, B. P., Bal, T., Tiwari, K., Hailu, Y. K., Sunita, S., Pravin, K. and Chandra, C., A review of emerging trends in nanomaterial-driven AI for biomedical applications, *Nanoscale Adv*., 7(12), 3619–3630(2025). https://doi.org/10.1039/D5NA00032G

Chou, W. C., Alexa, C., Zhang, F. and Lin, Z., Machine Learning and Artificial Intelligence in Nanomedicine, *WIREs Nanomed. Nanobiotechnol*., 17(4), 70027(2025). https://doi.org/10.1002/wnan.70027

Das, K. P. and Chandra, J., Nanoparticles and convergence of artificial intelligence for targeted drug delivery for cancer therapy: Current progress and challenges, *Front. Med. Technol*., 4, 1067144(2023). https://doi.org/10.3389/fmedt.2022.1067144

Day, A. L., Wahl, C. B., Dos, R. R., Liao, W. K., Dravid, V. P., Alok, C. and Ankit, A., Automated Nanoparticle Image Processing Pipeline for AI-Driven Materials Characterization, *Proce. 33rd ACM Int. Conf. Inform. Knowledge Manage.,* 4462–4469(2024). https://doi.org/10.1145/3627673.3680100

Eliasson, H., Angus, L., Ivan, S., Sharon, M., Javier, P. R. and Rolf, E., Precise Size Determination of Supported Catalyst Nanoparticles via Generative AI and Scanning Transmission Electron Microscopy, *Small Meth*., 9(3), (2025). https://doi.org/10.1002/smtd.202401108

Faraz, K., Thomas, G., Ducottet, C. and Epicier, T., Deep learning detection of nanoparticles and multiple object tracking of their dynamic evolution during in situ ETEM studies, *Sci. Rep.,* 12(1), 2484(2022). https://doi.org/10.1038/s41598-022-06308-2

Glaubitz, C., Amelie, B., Liliane, A. H., Laura, B., Moritz, H., Roman, F., Barbara, R. R., Balog, S., Alke, P. F., Leveraging Machine Learning for Size and Shape Analysis of Nanoparticles: A Shortcut to Electron Microscopy, *J. Phy. Chem. C*, 128(1), 421–427(2024). https://doi.org/10.1021/acs.jpcc.3c05938

Kim, H., Han, J. and Han, T. Y. J., Machine vision-driven automatic recognition of particle size and morphology in SEM images, *Nanoscale,* 12(37), 19461–19469(2020). https://doi.org/10.1039/D0NR04140H

Kirilov, A., Eric, M., Ravi, N., Mao, H., Chloe, R., Laura, G., Xiao, T., Spencer, W., Berg, A. C., Lo, W. Y., Piotr, D. and Ross, G., Segment anything, *arXiv[SPACE],* (2023). https://doi.org/10.48550/ arXiv.2304.02643

Larsen, R., Villadsen, T. L., Jette, K. M., Jensen, K. M. and Espen, B. D., NP-SAM: Implementing the Segment Anything Model for Easy Nanoparticle Segmentation in Electron Microscopy Images, (2023). https://doi.org/10.26434/chemrxiv-2023-k73qz-v2

LeCun, Y., Bengio, Y. and Hinton, G., Deep learning, *Nat.,* 521(7553), 436–444(2015). https://doi.org/10.1038/nature14539

Lin, S., Cui, L. and Ke, N., End-to-End Encrypted Message Distribution System for the Internet of Things Based on Conditional Proxy Re-Encryption, *Sens.,* 24(2), 438(2024). https://doi.org/10.3390/s24020438

Lin, Y. C., Elena, P., Lin, Z. R., Chang, C. C., Chen, H. H., Yang, S. M., Lin, M. D., Karmenyan, A., Giorgio, S., Luca, M., Nebel, C. and Cheng, C. L., Multimodal bioimaging using nanodiamond and gold hybrid nanoparticles, *Sci. Rep.,* 12(1), 5331(2022). https://doi.org/10.1038/s41598-022-09317-3

Matskevych, A., Wolny, A., Pape, C. and Anna, K., From Shallow to Deep: Exploiting Feature-Based Classifiers for Domain Adaptation in Semantic Segmentation, *Front. Comp. Sci.,* 4, 805166(2022). https://doi.org/10.3389/fcomp.2022.805166

Mim, J. J., Rakib, S., Akter, S., Nisha, J. R., Khan, S., Rahman, S. M. M., Manik, M. H. and Hossain, N., The emerging role of machine learning in nanomaterials research: applications, challenges, and future directions, *J. Nanopart. Res.,* 27(11), 282(2025). https://doi.org/10.1007/s11051-025-06472-2

Monteiro, G. A. A. and Wittemann, A., Linear growth of colloidal dumbbells into three-lobed polymer nanoparticles mediated by a gradient in surface wettability, *Colloid Polym. Sci.,* 301(7), 801–812(2023). https://doi.org/10.1007/s00396-023-05131-z

Monteiro, G. A. A., Bruno, M. A. A., Dos, S. J. A. and Wittemann, A., Pre-trained artificial intelligence-aided analysis of nanoparticles using the segment anything model, *Sci. Rep.,* 15(1), 2341(2025). https://doi.org/10.1038/s41598-025-86327-x

Nath, B. P., Saini, K. and Anand, P., AI-Driven Optimization of Nano-modified Bitumen: CO_2 reduction Efficiency Through Machine Learning and Optimization Framework, *Int. J. Pave. Res. Technol*., (2025). https://doi.org/10.1007/s42947-025-00593-6

Ruhle, B., Krumrey, J. F. and Hodoroaba, V. D., Workflow towards automated segmentation of agglomerated, non-spherical particles from electron microscopy images using artificial neural networks, *Sci. Rep.,* 11(1), 4942(2021). https://doi.org/10.1038/s41598-021-84287-6

Schulz, B., Haghdadi, N., Leitner, T., Hafok, M. and Primig, S., Advancing analytical electron microscopy methodologies to characterise microstructural features in superalloys, *Ultramicros.,* 247, 113699(2023). https://doi.org/10.1016/j.ultramic.2023.113699

Smits, H. J. G., Swartz, J. E., Philippens, M. E. P., De, B. R., Kaanders, J. H. A. M., Koppes, S. A., Gerben, B. E. and Stefan, W. M., Validation of automated positive cell and region detection of immunohistochemically stained laryngeal tumor tissue using digital image analysis, *J. Pathol. Inform.,* 14, 100198(2023). https://doi.org/10.1016/j.jpi.2023.100198

Tamilselvan, K., Aruna, S., Albert, J. R. and Kumar, R., Optimizing cloud service cryptography via fuzzy graph theory neural networks: A data model perspective, *AIP Adv.,* 15 (10), 105318(2025). https://doi.org/10.1063/5.0300303

Van, D. W. S., Schonberger, J. L.., Juan, N. I., Francois, B., Warner, J. D., Neil, Y., Gouillart, E. and Yu, T., Scikit-image: image processing in Python, *PeerJ*, 2, e453(2014). https://doi.org/10.7717/peerj.453

Wang, Q., Liu, Y., Li, C., Xu, B., Xu, S. and Liu, B., Machine Learning-Enhanced Nanoparticle Design for Precision Cancer Drug Delivery, *Adv. Sci.,* 12(30), e03138(2025). https://doi.org/10.1002/advs.202503138

Xu, H., Xing, Y. and Wang, W., Image segmentation with boundary-to-pixel direction and magnitude based on watershed and attention mechanism, *Signal, Image Video Processing*, 17(4),1695–1703(2023). https://doi.org/10.1007/s11760-022-02380-3

Yang, B., Ceri, R. J., Timea, B. G., De, B. I., Itxaso, A. Z., Else, N. and Aberg, C., Following nanoparticle uptake by cells using high-throughput microscopy and the deep-learning based cell identification algorithm Cellpose, *Front. Nanotechnol.,* 5, 1181362(2023). https://doi.org/10.3389/fnano.2023.1181362

Yildirim, B. and Cole, J. M., Bayesian Particle Instance Segmentation for Electron Microscopy Image Quantification, *J. Chem. Inform. Model.,* 61(3), 1136–1149(2021). https://doi.org/10.1021/acs.jcim.0c01455

Zhai, J., Yin, X., Jie, X., Du, P., Chen, W. H. and Song, L., Silicon/nickel oxide core/shell nanospheres as a hole transport layer for high efficiency and light-stable perovskite solar cells, *Phy. Chem. Chem. Phy.,* 25(20), 14056–14063(2023). https://doi.org/10.1039/D3CP00678F